

## A study of confined Stark effect, hydrostatic pressure and temperature on nonlinear optical properties in 1D $\text{Ga}_x\text{Al}_{1-x}\text{As}/\text{GaAs}/\text{Ga}_x\text{Al}_{1-x}\text{As}$ quantum dots under a finite square well potential

Rohit Chaurasiya, Suman Dahiya, Rinku Sharma

Department of Applied Physics, Delhi Technological University, Shahbad Daultpur, 110042, Delhi, India

Corresponding author: Rohit Chaurasiya, [rohitqc2000@gmail.com](mailto:rohitqc2000@gmail.com)

**ABSTRACT** In the present paper, investigations of nonlinear optical rectification, absorption coefficient and refractive index in a 1D  $\text{Ga}_x\text{Al}_{1-x}\text{As}/\text{GaAs}/\text{Ga}_x\text{Al}_{1-x}\text{As}$  quantum dots under a finite square well potential using simulation software such as COMSOL Multi-Physics and Matlab have been carried out in the presence of electric field, hydrostatic pressure and temperature. Results show that the resonant peaks of ORC (optical rectification coefficient) exhibit a blue shift under increasing of the electric field, while a red shift trailed by a blue shift is displayed under increasing of hydrostatic pressure and temperature. Similar trends take place for the refractive index as well as for the absorption coefficient under changing of the electric field, temperature and hydrostatic pressure. The attained theoretical results would pave a novel opportunity in designing, optimizing and applications of nonlinear opto-electronic devices by tuning the performance of the quantum dots and controlling some of their specific properties.

**KEYWORDS** confined Stark effect, quantum dot, second harmonic generation, third harmonic generation

**FOR CITATION** Chaurasiya R., Dahiya S., Sharma R. A study of confined Stark effect, hydrostatic pressure and temperature on nonlinear optical properties in 1D  $\text{Ga}_x\text{Al}_{1-x}\text{As}/\text{GaAs}/\text{Ga}_x\text{Al}_{1-x}\text{As}$  quantum dots under a finite square well potential. *Nanosystems: Phys. Chem. Math.*, 2023, **14** (1), 44–53.

### 1. Introduction

The broad range of applications of nano-scale semiconductors has piqued the interest of scientists from various fields. It has applications in quantum computing, photonic computing, photovoltaics, biomedicine, and other fields. At nanoscales, the potential barrier can be used to confine electrons and holes inside the potential well. These quantum systems are classified into three types based on the degree of confinement. When an electron is confined in all three dimensions, it is referred to as a quantum dot. When electrons are confined in two dimensions, they form quantum wires, and when they are confined in only one dimension, they form quantum layers (quantum wells in one dimension). All of these systems cause interesting changes in the nonlinear optical properties.

The quantum confined Stark effect is a well-known phenomenon that occurs when an electric field is added to a potential well. This phenomenon has piqued researchers to investigate the effect [1–4]. Two distinct characters of behaviour have been revealed. The electric field first induces bending and tilting of the material energy band structure. This has a direct impact on lowering electron energy, resulting in a red shift. The electric field also causes excitons to polarise. The electron and hole are pushed back, reducing the Coulomb force of attraction and increasing the energy of the electron-hole pair. As a result, the demand for non-linear crystals is increasing [5]. The study of optical behaviour in the presence of the electric field provides insight into the crystal controllability. This has prompted a slew of researchers to investigate these properties, as well as the impact of the electric field [6, 7].

There were numerous studies that showed the effect of field strength, temperature, and pressure on non-linear properties such as Optical Rectification Coefficient (ORC), Absorption Coefficient (AC), and change in Refractive Index (RI) in quantum dot systems including parabolic and semi-parabolic potentials [8, 9]. Observing these changes is crucial because these external factors can be used to tune and control nanoscale devices with quantum dots. The second harmonic generation was first reported experimentally by [10]. Since then, there were a plethora of simulation studies on these properties including different structures [5, 11, 12], and different potentials such as parabolic [14], semi-parabolic [13]. To the best of our knowledge, the work done on the study of non-linear optical properties, particularly for finite square well potential was not sufficient. The effect of an external electric field, pressure and temperature on optical rectification coefficient (ORC), Absorption coefficient (AC) and Refractive Index (RI) are discussed in 1D.

The band gaps of semiconductor materials can also be determined by the material's composition. The energy band of ternary semiconductors, for example, is determined by the composition of one of the elements in the compound.  $\text{Al}_x\text{Ga}_{1-x}\text{N}$  is one of the well-established materials used for UV light emitters and detectors [15] because of its wide band gap, which may span a wide range of wavelengths in this region. These materials' band structures are also affected by temperature and pressure. These variables have a significant impact on the fundamental properties of these materials

including the optoelectronic properties. Many semiconductor devices, such as QLEDs, Lasers, and white light sources, can benefit from the application of these external influences, which can improve the band structures of the material and, hence, boost efficiency [8].

The study starts with an overview of the methods used to run the simulations and compute the nonlinear features, as well as the state's wave functions and energy values. This section is followed by the problem's theoretical formulation. Following that, we present the findings and discuss them in the next section.

## 2. Theory and method

This work considers the quantum dot system of  $\text{Ga}_x\text{Al}_{1-x}\text{As}/\text{GaAs}$ . A 3D quantum well is created by sandwiching a nano cube of GaAs in a sea of  $\text{Ga}_x\text{Al}_{1-x}\text{As}$ . It is formed as a result of GaAs having a lower barrier potential than the surrounding material, which in our case is  $\text{Ga}_x\text{Al}_{1-x}\text{As}$ . When an external electric field is applied to a quantum dot system, the electron's energy tends to decrease. As a result, the allowed frequency of the light absorption or emission decreases. Correspondingly, drastic changes in nonlinear optical properties such as coefficient of absorptions and refractive index occur. Fig. 1(b) depicts the effect of the external electric field [16],  $E = -eFx$ . The potential level tilts by a slope of  $-eF$  in its application, where  $e$  is the charge of the electron.

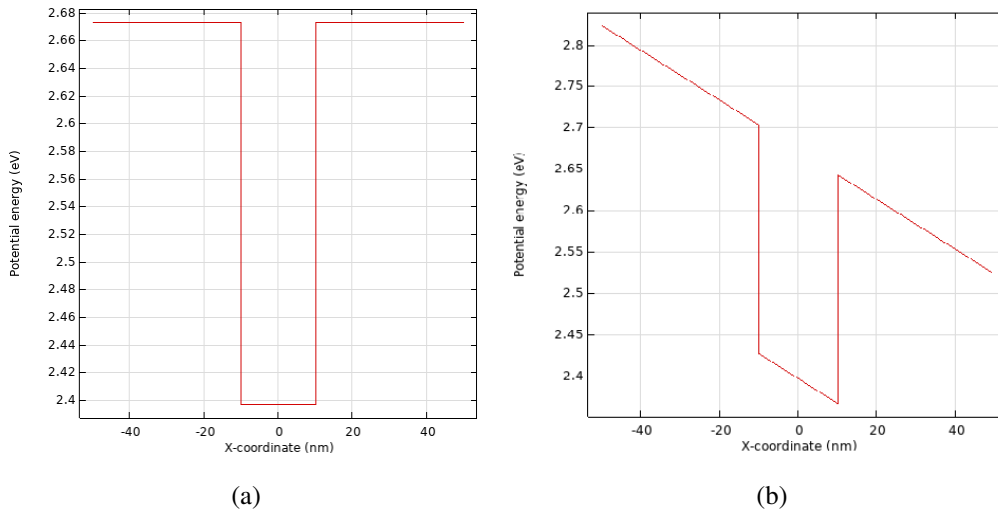


FIG. 1. Potential well of the system with the effect of a linearly varying external electric field: no electric field is applied (a); the application of the electric field (b)

### 2.1. Schrödinger equation for the system

Equation (1) gives the Schrödinger equation for the same system (considering only one dimension) in the presence of external electric field  $F$  for a single electron.

$$-\frac{\hbar^2}{2m_e^*} \frac{\partial^2 \psi}{\partial x^2} + (V_0 - eFx)\psi = E\psi, \quad (1)$$

where,

$$V_0 = \begin{cases} V_{\text{GaAs}} & -10 \text{ nm} \leq x \leq 10 \text{ nm}; \\ V_{\text{Ga}_x\text{Al}_{1-x}\text{As}} & \text{elsewhere.} \end{cases}$$

The effective mass of the electron is denoted by  $m_e^*$ . The pressure and temperature dependent effective electron mass has been calculated using the temperature and pressure dependent relation [17] for the GaAs region. It is expressed as eq. (2):

$$m_e^*(P, T) = m_e \left[ 1 + 7.51 \left( \frac{2}{E_g(P, T)} + \frac{1}{E_g(P, T) + \Delta_0} \right) \right]^{-1}. \quad (2)$$

The mass of the electron was calculated using eq. (3) for the region outside GaAs, which is the region of  $\text{Ga}_x\text{Al}_{1-x}\text{As}$ . The expression is a function of the fraction of Gallium mass in the semiconductor and the electron rest mass  $m_e$  [18]. For our investigation, the value of  $x$  has been set to zero.

$$m_e^* = (0.067 + 0.083(1 - x))m_e. \quad (3)$$

Similarly, the energy band gap for GaAs was calculated using the pressure and temperature dependence relation [19] given in eq. (4). While that for  $\text{Ga}_x\text{Al}_{1-x}\text{As}$ , eq. 5 was used.

$$E_g(P, T) = 1.519 - \frac{5.4 \times 10^{-4} T^2}{T + 204} + 0.01261P + 3.77 \times 10^{-5} P^2, \quad (4)$$

$$E_g = (1.426 + 1.247(1 - x)) \text{ eV}. \quad (5)$$

Equation (1) is a special differential equation and its solution comes in the form of Airy functions [20]. The detailed derivation for the analytical solution of eq. 1 can be found in [21]. The final form of the solution is expressed in eq. (6):

$$\psi = \begin{cases} A_1 \text{Ai}(x) + A_2 \text{Bi}(x) & -10 \text{ nm} \leq x \leq 10 \text{ nm}; \\ B_1 \text{Ai}(x) + B_2 \text{Bi}(x) & x \leq -10 \text{ nm}; \\ C_1 \text{Ai}(x) + C_2 \text{Bi}(x) & -10 \text{ nm} \leq x. \end{cases} \quad (6)$$

$A_i(x)$  and  $B_i(x)$  are the coefficients of the Airy functions. These coefficients are in integral form and henceforth, it becomes difficult to calculate exact solution and other parameter associated in the study. Due to this reason, numerical simulation was used to perform calculations.

## 2.2. Non-linear optical properties

The study takes into account non-linear properties such as absorption co-efficient and change in refractive index. This study addresses these properties by utilising a two-level system. The non-linear susceptibility is directly related to the coefficient of absorption and changes in the refractive index. Consider eq. (8) for the effective susceptibility with linear and non-linear terms.

$$\chi_{eff} = \chi^{(1)}E + \chi^{(2)}E^2 + \chi^{(3)}E^3, \quad (7)$$

$\chi^{(1)}$ ,  $\chi^{(2)}$  and  $\chi^{(3)}$  are linear, the second order, and the third order susceptibility terms that depend on the frequency of the falling radiation.  $\chi^{(2)}$  is made up of two terms: the optical rectification  $\chi^{(2)}(0)$  and the second harmonic generation  $\chi^{(2)}(2\omega)$ .

$$\chi^{(2)}(0) = \frac{4\sigma |M_{12}|^2 (M_{22} - M_{11})}{\epsilon \hbar^2} \left( \frac{\left( \omega_{12}^2 \left( 1 + \frac{\Gamma_1}{\Gamma_2} \right) + \left( w_p^2 + \frac{1}{\Gamma_2^2} \right) \right)}{\left( (\omega_{12} - \omega)^2 + \frac{1}{\Gamma_2^2} \right) \left( (\omega_{12} + \omega)^2 + \frac{1}{\Gamma_2^2} \right)} \right), \quad (8)$$

$$\chi_{2\omega}^{(2)} = \frac{\sigma}{\epsilon_0} \frac{M_{12} M_{23} M_{31}}{(\hbar\omega - E_{12} - j\hbar\Gamma_{21}) (2\hbar\omega - E_{31} - j\hbar\Gamma_{31})}. \quad (9)$$

Equations (8) and (9) were derived by using the density matrix approach [22].  $M_{ij}$  is the dipole transition element. It can be calculated by using the following expression:  $M_{fi} = -e \langle \psi_f | x | \psi_i \rangle$ , where,  $\psi_i$  and  $\psi_f$  are the initial and the final state wavefunction of the electron. The  $E_{ij}$  terms are the transition energy between  $i^{th}$  to  $j^{th}$  state. Finally,  $\sigma$  and  $\Gamma$  are the electron charge density and relaxation time, respectively.

The linear term of the coefficient of absorption is given by eq. (10). In the equation,  $\epsilon_0$  and  $\epsilon_R$  are the permittivity and the relative permittivity respectively.  $n_r$  is the relative refractive index of the material and  $I$  is the intensity of the electric field.

$$\alpha^{(1)}(\omega) = \omega \sqrt{\frac{\mu}{\epsilon_R}} \frac{|M_{21}|^2 \sigma_v \hbar \Gamma_{21}}{(E_{21} - \hbar\omega)^2 + (\hbar\Gamma_{21})^2}. \quad (10)$$

The non-linear term of AC is a function of the intensity of the incoming radiation and its frequency. It is expressed in eq. (11):

$$\alpha^{(3)}(I, \omega) = -\omega \sqrt{\frac{\mu}{\epsilon_R}} \left( \frac{I}{2\epsilon_0 n_r c} \right) \frac{|M_{21}|^2 \sigma_v \hbar \Gamma_{21}}{\left[ (E_{21} - \hbar\omega)^2 + (\hbar\Gamma_{21})^2 \right]^2} \times \left[ 4|M_{21}|^2 - \frac{|M_{22} - M_{11}|^2 [3E_{21}^2 - 4E_{21}\hbar\omega + \hbar^2(\omega^2 - \Gamma_{21}^2)]}{E_{21}^2 + (\hbar\Gamma_{21})^2} \right]. \quad (11)$$

The total coefficient of absorption can be written as the sum of linear and non-linear terms [23].

$$\alpha(I, \omega) = \alpha^{(1)}(\omega) + \alpha^{(3)}(I, \omega). \quad (12)$$

Similarly, the change in RI can be given as the sum of linear and non-linear parts as shown in eq. (13). The linear part is given by eq. (14) and the non-linear term is expressed as eq. (15):

$$\frac{\Delta n(\omega)}{n_r} = \frac{\Delta n^{(1)}(\omega)}{n_r} + \frac{\Delta n^{(3)}(\omega)}{n_r}, \quad (13)$$

$$\frac{\Delta n^{(1)}(\omega)}{n_r} = \frac{\sigma_v |M_{21}|^2}{2n_r^2 \varepsilon_0} \left[ \frac{E_{21} - \hbar\omega}{(E_{21} - \hbar\omega)^2 + (\hbar\Gamma_{21})^2} \right], \quad (14)$$

$$\frac{\Delta n^{(3)}(\omega)}{n_r} = -\frac{\mu c}{4n_r^3 \varepsilon_0} |M_{21}|^2 \left[ \frac{\sigma I}{E_{21} - \hbar\omega} (E_{21} - \hbar\omega)^2 + (\hbar\Gamma_{21})^2 \right]^2 \times \left[ 4(E_{21} - \hbar\omega) |M_{21}|^2 - \frac{(M_{22} - M_{11})^2}{(E_{21})^2 + (\hbar\Gamma_{21})^2} \left\{ (E_{21} - \hbar\omega) \times [E_{21}(E_{21} - \hbar\omega) - (\hbar\Gamma_{21})^2] - (\hbar\Gamma_{21})^2 (2E_{21} - \hbar\omega) \right\} \right]. \quad (15)$$

### 2.3. Method

To solve the Schrödinger equation in 1D, we used the finite elements method with the help of COMSOL Multi-physics. In the regions of different materials and at the boundary, suitable conditions such as mass approximation and zero probability conditions were used. The wavefunction and the eigenenergy values for eq. (1) are shown in Fig. 2. The thickness of the GaAs is set at 20 nm, with values ranging from 10 to  $-10$  nm. Using the finite element method, the numerical values of the wavefunctions were used to calculate the transition dipole matrix element. Matlab simulation software was used to perform this calculation.

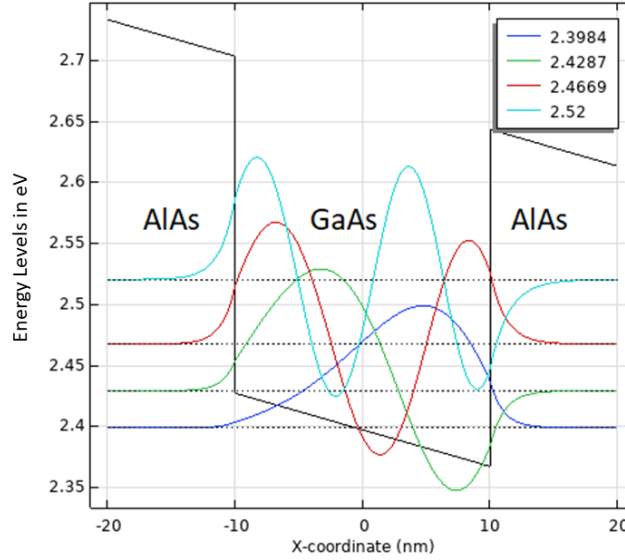


FIG. 2. Wavefunction of electron till 4<sup>th</sup> level. Here the y-axis shows the energy levels of the wavefunction

### 3. Result and discussion

This section presents the results of the simulations for varying electric fields, hydrostatic pressure and temperature strength at  $5k$  V/cm fixed intervals. Table 1, displays the list of fixed parameters as well as the values used to run the simulation. The values for relaxation time are as follows:  $\tau_{31} = \tau_{21}/2$  and  $\tau_{41} = \tau_{21}/3$ . The transition dipole matrix elements were calculated using the numerical wavefunctions obtained from the simulation. The matrix is important because all of the simulation results are related to its elements.

Parameters	Values
electron charge density ( $\sigma$ )	$2.8 \times 10^{22} \text{ m}^{-3}$
incident intensity ( $I$ )	$4 \times 10^6 \text{ W/m}^2$
relative refractive index ( $n_r$ )	3.2
relaxation time ( $\tau_{21}$ )	$0.5 \text{ ps}^{-1}$

TABLE 1. Table for Parameters and Values

Optical Rectification Coefficient or ORC, with the variation of the electric field in the interval of 25 kV/cm keeping temperature and pressure constant at 50 K and 100 kbar, respectively, for the system under consideration, is depicted in Fig. 3(a). Fig. 3(b) demonstrates energy eigenvalues for different values of the external electric field  $F$ . It can be observed from the figure that while increasing the electric field ORC peaks decrease in magnitude and shift towards higher frequencies, hence exhibiting a blue shift. As we can observe from Fig. 3(b) the increasing electric field strength leads to the increase of the energy eigenvalue, hence, an increase in the electric field lead to increase of the difference between energy levels leading to the blue shift.

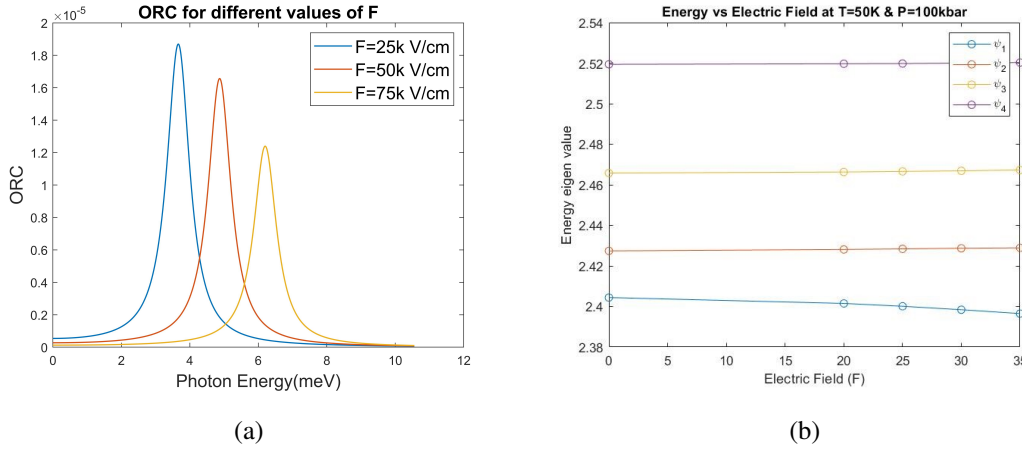


FIG. 3. (a) ORC for different values of electric field strength keeping temperature and hydrostatic pressure constant. (b) Energy eigenvalue vs electric field strength

Figure 4(a) shows a plot of ORC vs temperature at three diverse values fixing  $P = 50\text{ kbar}$ , electric field strength = 25 kV/cm. Blue shift is observed with an increase in the temperature as the resonant peaks move towards higher energy domain with significant decrease in the peak height. As the transition energy goes to increase with the increase in temperature, the blue shift happens. Also, with an increase in temperature, a decrease in the effective radius of the quantum dot is observed due to an enhancement in the effective electron mass as well an increase in energy interval is observed with an increase in the temperature.

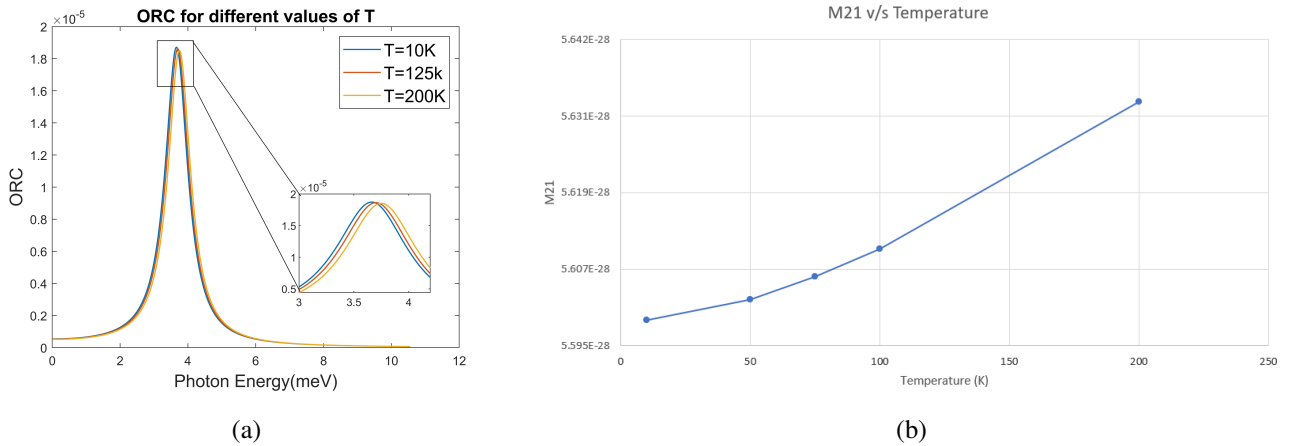
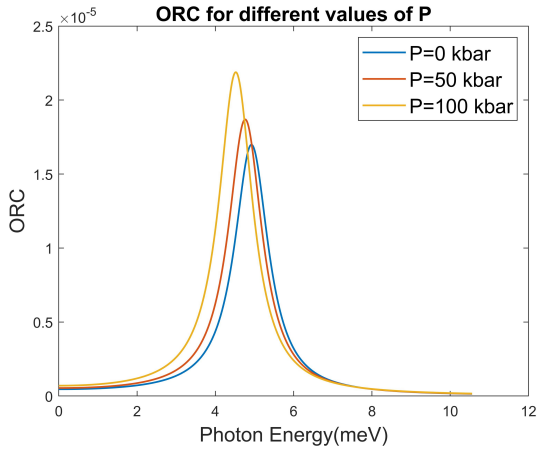


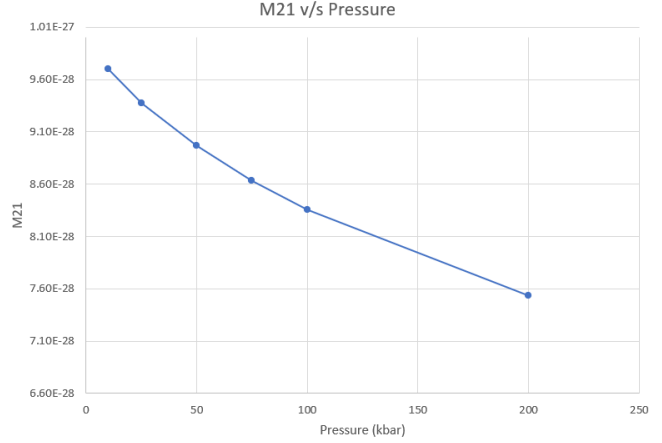
FIG. 4. (a) ORC for diverse values of temperature keeping the strength of the field and hydrostatic pressure constant. (b) matrix element vs temperature

Figure 5(a) shows a plot of ORC vs pressure at three different values fixing  $T = 50\text{ K}$ , the electric field strength equals to 25 kV/cm. It is observed that with an increase in the hydrostatic pressure the red shift is observed with the movement of resonant peaks towards higher energy domain with a substantial increase in the peak heights. This is due to the weakness of the quantum confinement with the decrease in the energy interval with a rise in hydrostatic pressure.

Figure 6(a) shows the first and the third order coefficients of absorption for different values of the electric field strength while keeping the temperature and the hydrostatic pressure constant, whereas Fig. 6(b) shows the total coefficients of absorption for different values of the electric field strength while keeping the temperature and the hydrostatic pressure constant. The total coefficient of absorption was displayed for various values of the electric field strength while keeping



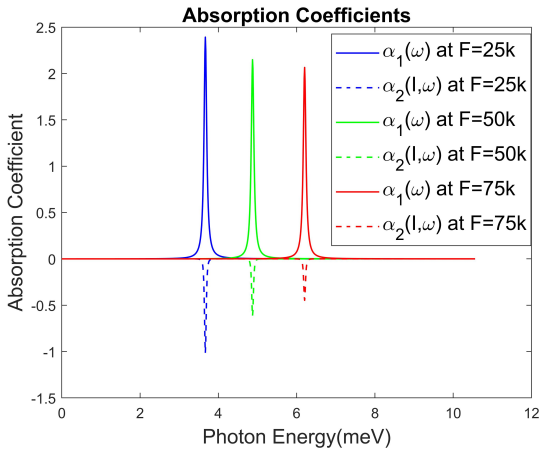
(a)



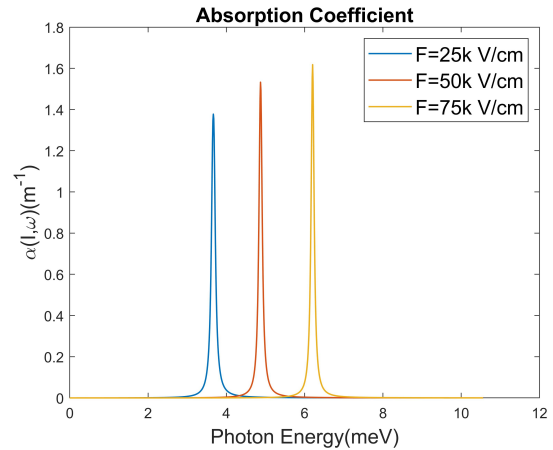
(b)

FIG. 5. (a) ORC for various values of hydrostatic pressure while maintaining constant electric field and temperature. (b) dipole transition  $M_{21}$  vs pressure

the temperature and the hydrostatic pressure constant. As can be seen in the figures, the linear coefficient of absorption decreases in amplitude as the electric field increases, while the nonlinear term remains nearly constant. As a result, this slight decrease in the linear coefficient of absorption also tries to reduce the total coefficient of absorption. It is also noticed that an increase in the electric field causes the peak positions to move towards lower photon energies, resulting in a red shift since the difference between energy levels decreases as the electric field increases.



(a)



(b)

FIG. 6. (a) 1<sup>st</sup> and 3<sup>rd</sup> order coefficient of absorption for diverse values of strength of the electric field keeping the temperature and the hydrostatic pressure constant. (b) The total coefficient of absorption for various field strength keeping temperature and hydrostatic pressure constant

In Fig. 7(a), the coefficient of absorption, for temperature values of 10, 100 and 200 K keeping the electric field and the hydrostatic pressure constant, was plotted. In Fig. 7(a), maximum values for the 1<sup>st</sup> order and the 3<sup>rd</sup> (nonlinear term) absorption coefficients were plotted while the sum of both the terms, with variation of temperature  $T$ , were plotted in Fig. 7. We can observe that the magnitude of the maximum value for the first order AC is increasing with an increase in the temperature as well as peaks are shifting towards higher energy depicting a blue shift. As shown in Fig. 7, as the temperature rises, the maximum values of the total ACs rise, demonstrating that temperature  $T$  influences intersubband optical absorption in QD. Furthermore, because the first and the third-order nonlinear ACs are diametrically opposed, the total ACs will be lowered, owing to the decrease in the effective mass of the electron with the rise in the temperature. The graphs reveal direct relationship between the peak values of the total ACs, the transition dipole element and the difference between energy levels  $E_{10}$ . The influence of the dipole matrix element  $|M_{21}|^2$  on the total ACs, on the other hand, is shown to be opposite that of the energy difference  $E_{10}$ . The second significant result depicted in the graph is the blue shift that occurs as the temperature  $T$  rises, which is due to a rise in the transition energy  $E_{10}$  as the temperature increases,

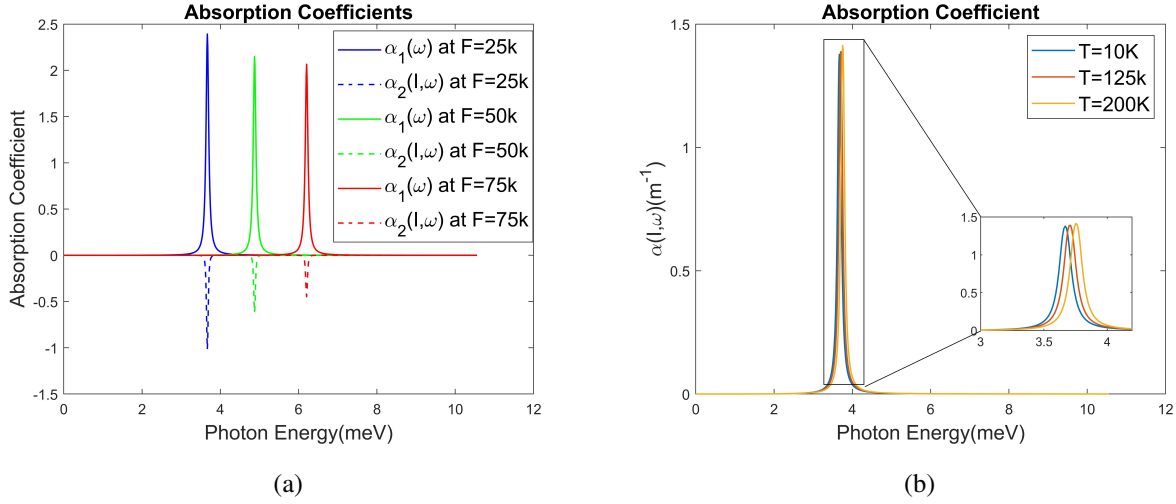


FIG. 7. (a)  $1^{st}$  and  $3^{rd}$  order coefficient of absorption for different values of temperature strength keeping the electric field and the hydrostatic pressure constant. (b) The total coefficient of absorption for different values of the temperature strength keeping the electric field and the hydrostatic pressure constant

resulting in a drop in the electron effective mass, and in an expansion of the transition energy. It happens because of the electron-photon interaction which depends on the temperature as well.

In Fig. 8(a), the coefficient of absorption for different values of the hydrostatic pressure strength keeping the electric field and the temperature constant was plotted. We can observe that the first order linear coefficient of absorption, as well as the total coefficient of absorption, show a red shift as the peaks move towards lower energies while increasing the pressure. It can also be observed that the magnitude of peaks is also diminishing with the increase in the pressure. As the linear  $\alpha_1(\omega)$ , the third-order nonlinear  $\alpha_3(\omega)$  are opposite in sign, hence the magnitude of the total coefficient of absorption is also reduced subsequently. The main rationale for this behaviour is as follows: when the hydrostatic pressure rises, so does the electron effective mass, resulting in a slight weakening of the strength of confinement. Furthermore, because the peak intensity is proportional to the dipole matrix element  $|M_{21}|^2$  and the energy difference, the energy difference grows as hydrostatic pressure rises. Additionally, because strain is directly related to the variety of energy levels, the hydrostatic pressure causes the lattice constant to change. As a result, the strain fluctuates, decrease the first excited state.

In Fig. 9(a), the refractive index for various values of the field strength keeping the temperature and the pressure constant was plotted. The 1st order linear refractive index, as well as the total refractive index, show the same behaviour

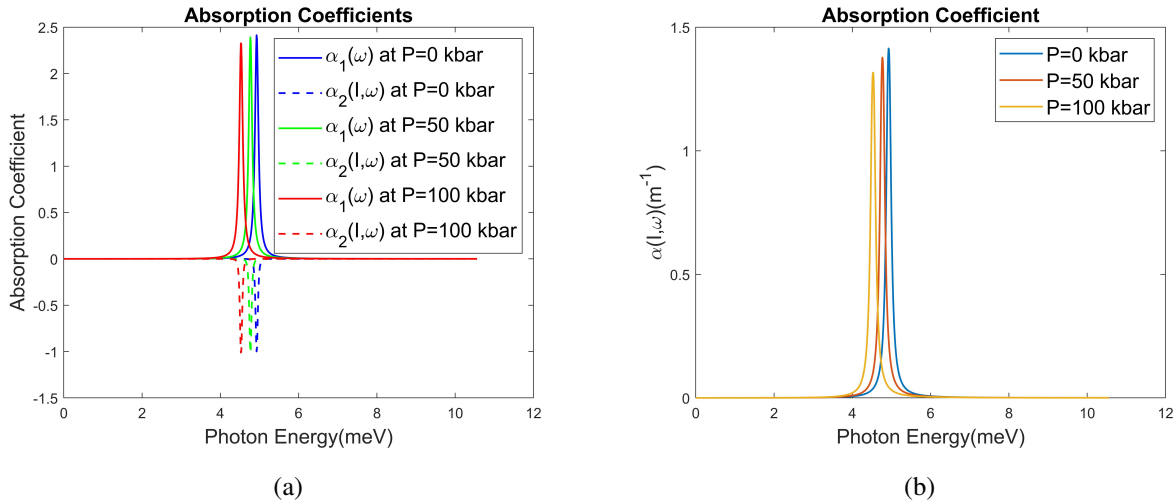


FIG. 8. (a) the  $1^{st}$  and The  $3^{rd}$  order coefficient of absorption for varied hydrostatic pressure keeping the strength of the field and the temperature constant. (b) The total coefficient of absorption for different values of the hydrostatic pressure strength keeping the electric field and the temperature constant

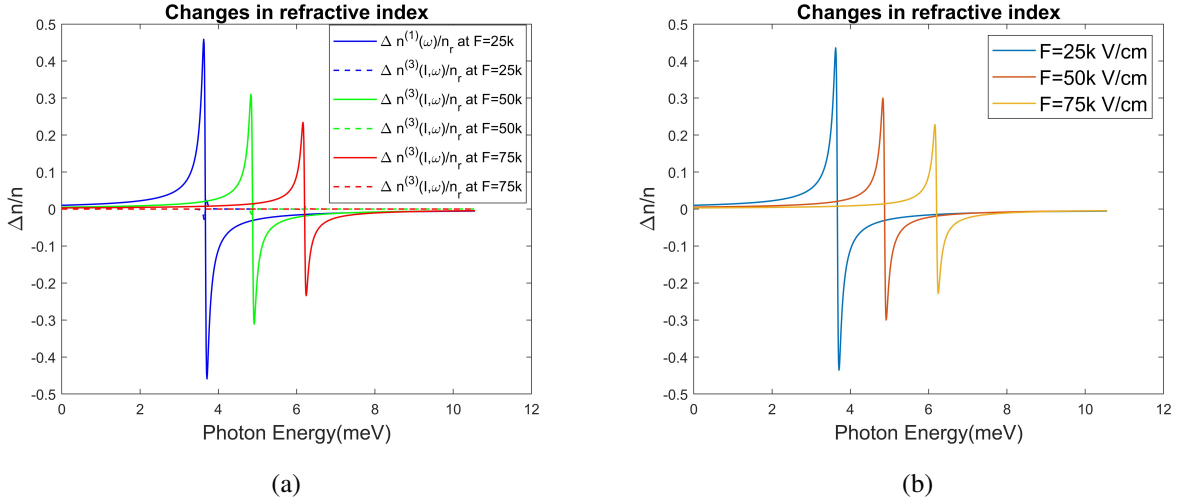


FIG. 9. (a)  $1^{st}$  and  $3^{rd}$  order refractive index for various values of electric field keeping temperature and pressure constant. (b) Total refractive index for various values of strength of the electric field keeping Temperature and Hydrostatic Pressure constant

with an increase in the electric field, as seen in Figs. 9(a) and 9(b), while the 3rd order non-linear term has no effect on the total refractive index due to its minimal contribution. It is observed that the magnitude of peaks is decreasing with an increase in the electric field while going towards a high energy state resulting in the blue shift.

In Fig. 10(a), the refractive index for various values of the temperature keeping the strength of the field and the hydrostatic pressure constant, was plotted. It can be observed from Fig. 10(b) that the 1st order linear refractive index, as well as the total refractive index, result in quite similar behaviour as we increase temperature although there is no noticeable effect in the 3rd order non-linear term hence observing a similar trend in peaks for both the 1st and the total refractive index due to neglecting the low contribution of the 3rd order non-linear term. A blue shift can be observed from the graphs as the peaks are moving towards a higher energy region with a significant increase in the peak height.

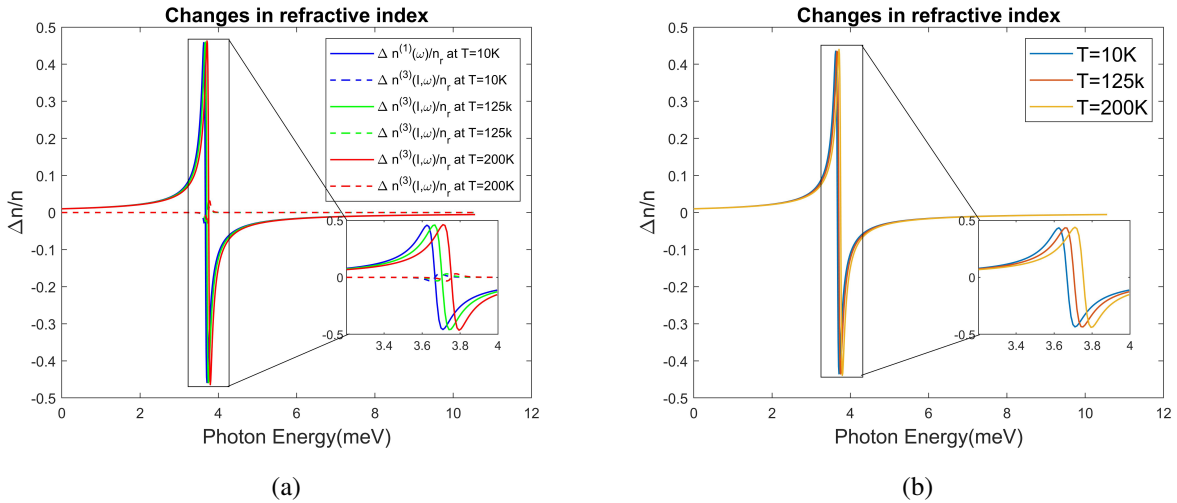


FIG. 10. (a) The  $1^{st}$  and the  $3^{rd}$  order refractive index for various temperature while maintaining the electric field and the hydrostatic pressure constant (b) The total refractive index at various temperature while the strength of the field and the hydrostatic pressure are held constant

In Fig. 11(a), the refractive index was plotted for various values of the hydrostatic pressure while maintaining the field strength and the hydrostatic pressure constant. Figs. 11(a) and 11(b) result in quite similar behaviour in both of the 1st order linear refractive index as well as the total refractive index with a significant increase in the hydrostatic pressure with no alteration although in the 3rd order non-linear term. Hence, we observe that the 1st order linear refractive index and the total refractive index are similar in magnitude as well as they exhibit the red shift with an increase in the magnitude of the peaks intensity.

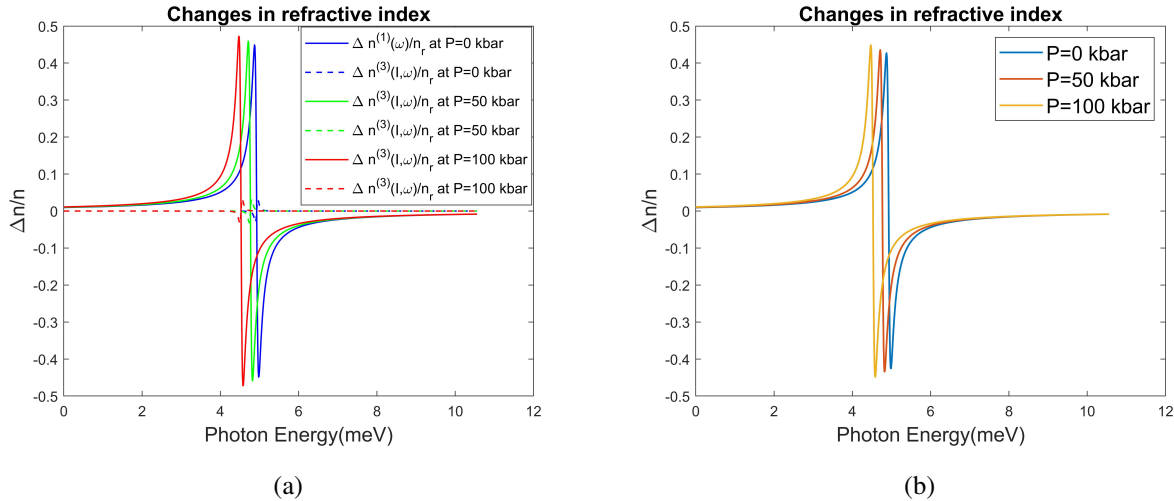


FIG. 11. (a) The 1<sup>st</sup> and the 3<sup>rd</sup> order refractive index for various hydrostatic pressure strengths while maintaining the electric field and the temperature constant (b) Total refractive index for various Hydrostatic pressure strengths while keeping the electric field and temperature constant

#### 4. Conclusion

We reported the variation of optical properties as a function of the external applied electric field, hydrostatic pressure and temperature in this study. The results show that increasing the field strength causes a red shift in all of the optical properties studied as well as a surge can be seen in the peak's intensity with an increase in the electric field. Furthermore, the simulation results show that the temperature causes a blue shift in the optical properties while hydrostatic pressure causes a redshift in the optical properties. As a result, the hydrostatic pressure  $P$ , temperature  $T$ , and applied electric field  $E$  all have a significant impact on the system's optical response.

#### References

- [1] Aderras L., et al. Stark-shift of impurity fundamental state in a lens shaped quantum dot. *Physica E: Low-dimensional Systems and Nanostructures*, 2017, **89**, P. 119–123.
- [2] Temkin H., et al.  $\text{Ge}_x\text{Si}_{1-x}$  strained-layer heterostructure bipolar transistors. *Applied Physics Letters*, 1988, **52** (13), P. 1089–1091.
- [3] Luryi S., Kastalsky A., Bean J.C. New infrared detector on a silicon chip. *IEEE Transactions on Electron Devices*, 1984, **31** (9), P. 1135–1139.
- [4] Rhee S.S., et al. Resonant tunneling through a  $\text{Si}/\text{Ge}_x\text{Si}_{1-x}/\text{Si}$  heterostructure on a GeSi buffer layer. *Applied Physics Letters*, 1988, **53** (3), P. 204–206.
- [5] Mohamed Kria Varsha, et al. Quantum Confined Stark Effect on the Linear and Non-linear Optical Properties of SiGe/Si Semi Oblate and Prolate Quantum Dots Grown in Si Wetting Layer. *Nanomaterials*, 2021, **11** (6).
- [6] Mourad Baira, et al. Intersubband optical nonlinearity of GeSn quantum dots under vertical electric field. *Micromachines*, 2019, **10** (4), 243.
- [7] Dvovyan K.G., Kazaryan E.M. Impurity states in a weakly prolate (oblate) ellipsoidal microcrystal placed in a magnetic field. *Physica Status Solidi B*, 2001, **228** (3), P. 695–703.
- [8] Suman Dahiya, Siddhartha Lahon, Rinku Sharma. Effects of temperature and hydrostatic pressure on the optical rectification associated with the excitonic system in a semi-parabolic quantum dot. *Physica E: Low-dimensional Systems and Nanostructures*, 2020, **118**, 113918.
- [9] Amal Abu Alia, Mohammad K. Elsaid, Ayham Shaer. Magnetic properties of GaAs parabolic quantum dot in the presence of donor impurity under the influence of external tilted electric and magnetic fields. *J. of Taibah University for Science*, 2019, **13** (1), P. 687–695.
- [10] Franken P.A., et al. Generation of optical harmonics. *Physical Review Letters*, 1961, **7** (4), 118.
- [11] Keyin Li, Kangxian Guo, Litao Liang. Effect of the shape of quantum dots on the refractive index changes. *Physica B: Condensed Matter*, 2016, **502**, P. 146–150.
- [12] Khaledi-Nasab A., et al. Optical rectification and second harmonic generation on quasi-realistic InAs/GaAs quantum dots: with attention to wetting layer effect. *Int. Scholarly Research Notices*, 2013 (2013).
- [13] Jin-Feng You, et al. The effect of temperature, hydrostatic pressure and magnetic field on the nonlinear optical properties of AlGaAs/GaAs semi-parabolic quantum well. *Int. J. of Modern Physics B*, 2019, **33** (27), 1950325.
- [14] Yuan Lihua, et al. Effect of a magnetic field on the energy levels of donor impurities in the ZnO parabolic quantum well. *J. of Semiconductors*, 2011, **32** (8), 082001.
- [15] Gil B. *Group III nitride semiconductor compounds: physics and applications*. Clarendon Press, 1998.
- [16] Empedocles S.A., Bawendi M.G. Quantum-confined Stark effect in single CdSe nanocrystallite quantum dots. *Science*, 1997, **278** (5346), P. 2114–2117.
- [17] Zaiping Zeng, et al. Competition effects of electric and magnetic fields on impurity binding energy in a disc-shaped quantum dot in the presence of pressure and temperature. *Science of Advanced Materials*, 2014, **6** (3), P. 586–591.
- [18] Harrison P., Valavanis A. *Quantum wells, wires and dots: theoretical and computational physics of semiconductor nanostructures*. John Wiley and Sons, 2016.
- [19] Aghoutane N., et al. Refractive index changes and optical absorption involving 1s1p excitonic transitions in quantum dot under pressure and temperature effects. *Applied Physics A*, 2019, **125** (1).

- [20] Vallee O., Soares M. *Airy functions and applications to physics*. World Scientific Publishing Company, Singapore, 2010.
- [21] Ghatak A.K., Goyal I.C., Gallawa R.L. Mean lifetime calculations of quantum well structures: a rigorous analysis. *IEEE J. of Quantum Electronics*, 1990, **26** (2), P. 305–310.
- [22] Boyd R.W. *Nonlinear optics*. Academic press, NY, 2020.
- [23] Rezaei G., Karimi M.J., Keshavarz A. Excitonic effects on the nonlinear intersub-band optical properties of a semi-parabolic one-dimensional quantum dot. *Physica E: Low-dimensional Systems and Nanostructures* 43 (1) (2010), pp. 475–481.

---

*Submitted 21 September 2022; revised 22 November 2022; accepted 23 November 2022*

*Information about the authors:*

*Rohit Chaurasiya* – Department of Applied Physics, Delhi Technological University, Shahbad Daulatpur, Main Bawana Road, Delhi, 110042, Delhi, India; rohitqc2000@gmail.com

*Suman Dahiya* – Department of Applied Physics, Delhi Technological University, Shahbad Daulatpur, Main Bawana Road, Delhi, 110042, Delhi, India; ORCID 0000-0003-4815-5354; dahiyasuman90@gmail.com

*Rinku Sharma* – Department of Applied Physics, Delhi Technological University, Shahbad Daulatpur, Main Bawana Road, Delhi, 110042, Delhi, India; ORCID 0000-0001-6812-4358; rinkusharma@dtu.ac.in

*Conflict of interest:* the authors declare no conflict of interest.